Korth, B., Pereira, J., Sleutels, T., **Harnisch, F.**, ter Heijne, A. (2023):
Comparing theoretical and practical biomass yields calls for revisiting thermodynamic growth models for electroactive microorganisms
Water Res. **242** , art. 120279

https://doi.org/10.1016/j.watres.2023.120279

Comparing theoretical and practical biomass yields calls for revisiting thermodynamic growth models for electroactive microorganisms

Benjamin Korth[a,*], João Pereira[b,c], Tom Sleutels[b,d], Falk Harnisch[a], Annemiek ter Heijne[c]

[a] Department of Environmental Microbiology, Helmholtz-Centre for Environmental Research, Permoserstr. 15, 04318 Leipzig, Germany

[b] Wetsus, European Centre of Excellence for Sustainable Water Technology, Oostergoweg 9, 8911MA, Leeuwarden, The Netherlands

[c] Environmental Technology, Wageningen University, Bornse Weilanden 9, P.O. Box 17, 6700 AA, Wageningen, The Netherlands

[d] Faculty of Science and Engineering, University of Groningen, Nijenborgh 4, 9747 AG, Groningen, The Netherlands

* Corresponding author: Benjamin Korth, benjamin.korth@ufz.de

Abstract

Research on electroactive microorganisms (EAM) often focuses either on their physiology and the underlying mechanisms of extracellular electron transfer or on their application in microbial electrochemical technologies (MET). Thermodynamic understanding of energy conversions related to growth and activity of EAM has received only a little attention. In this study, we aimed to prove the hypothesized restricted energy harvest of EAM by determining biomass yields by monitoring growth of acetate-fed biofilms presumably enriched in *Geobacter*, using optical coherence tomography, at three anode potentials and four acetate concentrations. Experiments were concurrently simulated using a refined thermodynamic model for EAM. Neither clear correlations were observed between biomass yield and anode potential nor acetate concentration, albeit the statistical significances are limited mainly due to the observed experimental variance. The experimental biomass yield based on acetate consumption ($Y_{\mathrm{X/ac}}$ = 37 ±9 $\mathrm{mgCOD_{biomass}\ gCOD_{ac}^{-1}}$) was higher than estimated by modeling, indicating limitations of existing growth models to predict yields of EAM. In contrast, the modeled biomass yield based on catabolic energy harvest was higher than the biomass yield from experimental data ($Y_{\mathrm{X/cat}}$ = 25.9 ±6.8 $\mathrm{mgCOD_{biomass}\ kJ^{-1}}$), supporting restricted energy harvest of EAM and indicating a role of, so far, not considered energy sinks. This calls for an adjusted growth model for EAM, including, e.g., the microbial electrochemical Peltier heat to improve the understanding and modeling of their energy metabolism. Furthermore, the reported biomass yields are important parameters to design strategies for influencing the interactions between EAM and other microorganisms and allowing more realistic feasibility assessments of MET.

Keywords

electroactive microorganisms, extracellular electron transfer, thermodynamic modeling, biomass yield, restricted energy harvest, microbial electrochemical technologies

1. Introduction

Electroactive microorganisms (EAM) extend their electron transfer chain across the periplasm and the outer membrane – this is called extracellular electron transfer (EET) (Kumar et al., 2017). EET allows coupling oxidation of soluble substrates, being electron donors (ED), to solid terminal electron acceptors (TEA). Hence, the energy harvesting metabolism is wired to the reduction of solid electron conductors that cannot pass the cellular envelope. EAM can also receive electrons from solid ED to perform reduction reactions using soluble TEA. In addition to using direct EET that needs physical contact, EAM are also known to use soluble redox shuttles (i.e., mediated EET) and to exchange electrons among each other (i.e., direct interspecies electron transfer, DIET) (Logan et al., 2019).

Exploiting a wide variety of insoluble ED and TEA is advantageous for EAM as it enables survival in ecological niches that are not accessible to other microorganisms (Koch and Harnisch, 2016). Following this unique physiological trait, a substantial influence of EAM on environmental processes seems evident including degradation of organic matter, redox cycling of metals (Gescher and Kappler, 2012), and biocorrosion (Dou et al., 2021). Moreover, EAM are discussed to be harnessed as bioelectrocatalyst in primary microbial electrochemical technologies (MET) for different applications (e.g., wastewater treatment, synthesis of chemicals, and desalination), with the technical devices being termed bioelectrochemical systems (BES) (Cao et al., 2009; Logan and Rabaey, 2012; Schröder et al., 2015). In BES, anode and cathode serve as inexhaustible electron sink (i.e., TEA) or electron source (i.e., ED), respectively. EAM exhibit planktonic and sessile growth, but the most efficient EAM for current production, *Geobacter sulfurreducens*, forms electroactive biofilms at electrodes (Malvankar et al., 2012).

During the last two decades, much research has focused on the physiology of EAM and the fundamentals of EET (Kumar et al., 2017; Logan et al., 2019). This interest has been driven by the desire to leverage the application potential of EAM and to reveal their actual impact on environmental processes. Surprisingly, knowledge of the thermodynamics of EET and energy conversions of EAM is still in its infancy. At the same time, these are central aspects when analyzing and predicting growth and activity of EAM. As thermodynamics determines the energetic limits of biological conversions, it represents a cornerstone for energetic and economic assessments of biotechnological processes (Kontogeorgis and Folas, 2010; von Stockar, 2018).

A first theoretical framework for thermodynamic analyses of MET on the system level was proposed by Sadhukhan et al. performing substrate screening for microbial fuel cells (MFC) and energy efficiency estimations for microbial electrochemical syntheses (Sadhukhan et al., 2016). One of the first experimental attempts to investigate the thermodynamics of EAM and the energetic consequences of EET was conducted in a combined experimental and constraint-based modeling study with planktonic cultures of the electroactive model organism *Geobacter sulfurreducens*. Comparing growth of *G. sulfurreducens* with soluble fumarate and insoluble Fe(III) as TEA revealed that biomass yield was significantly lower in case of Fe(III), suggesting a restricted catabolic energy harvest when EET is performed (Mahadevan et al., 2006). Recently, applying a thermodynamic model for EAM demonstrated that the catabolic energy harvest does not linearly correlate with the anode potential (i.e., the external driving force for EET) but exhibits a saturation effect (Korth and Harnisch, 2019). The maximum catabolic energy that can be used for generating proton motive force (*pmf*), which in turn is utilized for ATP synthesis (i.e., biological energy transduction), is not determined by the energy difference between the soluble ED and the solid TEA (including anodes). It is determined by the energy difference between the soluble ED and the last component of the electron transport chain that still contributes to *pmf* (Bird et al., 2011; Korth and Harnisch, 2019) (Figure 1a). However, it was not yet experimentally demonstrated that the energy harvest of EAM using anodes as TEA is limited and that a different theoretical approach is required for calculating the catabolic energy gain compared to microorganisms using soluble EA. One crucial obstacle for such an investigation is the need for a non-invasive and robust tool to monitor the biomass growth of electroactive biofilms at electrodes.

Recently optical coherence tomography (OCT) was introduced as biomass quantification method, which fulfills these requirements and allows corresponding experiments (Molenaar et al., 2018). OCT uses near-infrared light to visualize biofilm morphology and quantify the total biomass amount on electrodes at different time points. With this visual and non-invasive technique, the development of electroactive biofilms and their morphological adaptations can be studied at a micrometer resolution under different operating conditions. Thus, combining OCT measurements for assessing biomass production with quantification of the reactants of the catabolic reaction and thermodynamic modeling allows to investigate the restricted catabolic energy harvest.

To provide an experimental assessment of the hypothesis of restricted energy harvest of EAM using anodes as TEA, anodic electroactive biofilms were cultivated with different acetate concentrations and at different anode potentials. Concurrently, biomass production was monitored via OCT, and the biomass yield was calculated based on the consumed acetate and the harvested catabolic energy, assuming restricted energy harvest. In addition, a previously developed thermodynamic model for EAM (Korth et al., 2015) was refined and adapted to simulate the performed experiments. Experimental and model results indicate that the energy harvest of EAM is indeed restricted, but further experiments are required to decipher the relationship between biomass yield and acetate concentration or anode potential. Furthermore, it appears that established microbial growth models need adaptations to correctly simulate the thermodynamics of EAM.

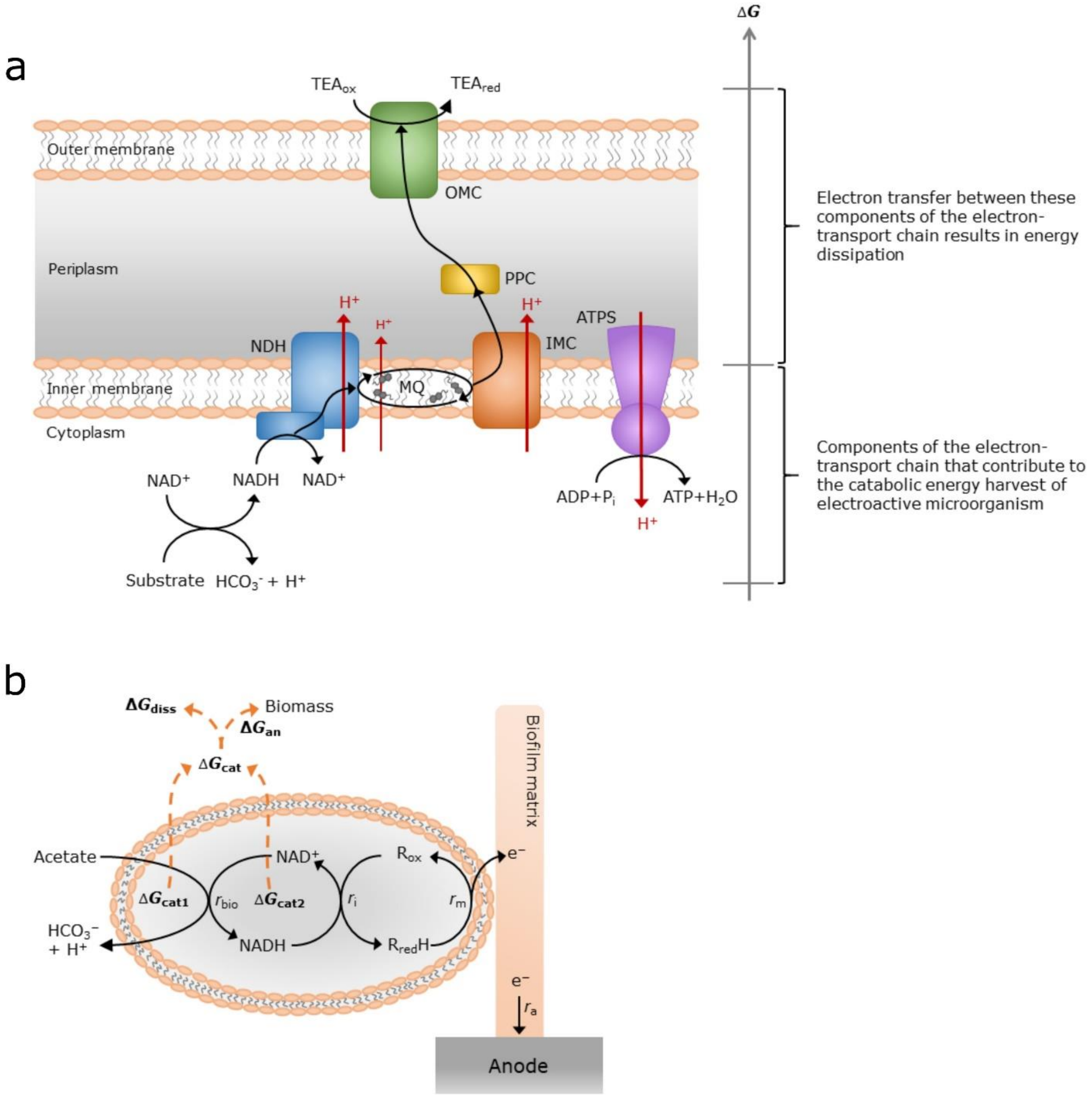

Figure 1 The restricted energy harvest of electroactive microorganisms (EAM). a) Simplified electron-transport chain of EAM illustrating the share of the energy difference between substrate and terminal electron acceptor (TEA) that EAM can utilize. During substrate oxidation, NADH is produced, which is oxidized by a NADH dehydrogenase (NDH) so that the electrons derived from the catabolic reaction enter the electron transport chain. Subsequently, electrons are transported via the menaquinone pool (MQ), inner membrane cytochromes (IMC), periplasmic cytochromes (PPC), and outer membrane cytochromes (OMC) to TEA. Only the energy difference between substrate and IMC is utilized as only these components can contribute to the proton gradient that is subsequently used by the ATP synthase (ATPS) for the generation of ATP. The energy difference between IMC and TEA cannot be exploited by electroactive microorganisms and is dissipated as heat as the involved components of the electron-transport chain cannot physically contribute to the proton gradient. b) Main biochemical and electrochemical reactions that occur at the cellular level of the enhanced thermodynamic model for electroactive microorganisms on the example of

Geobacter species oxidizing acetate. Thereby, the restricted catabolic energy harvest is simulated. Acetate oxidation is coupled to NAD$^+$ reduction (reaction rate r_{bio}), and the electrons are further transferred to redox centers (R_{ox}/$R_{\text{red}}H$) located at the inner membrane with the rate r_i. The Gibbs energy of both reactions (ΔG_{cat1} and ΔG_{cat2}) form the total catabolic energy harvest (ΔG_{cat}) that is subsequently used for the formation of biomass (ΔG_{an}) and for providing driving force for growth (i.e., dissipation energy, ΔG_{diss}). From redox centers, the electrons are transferred to the extracellular conductive biofilm matrix (r_m), which collects all electrons from all cells of all biofilm layers. All electrons are finally transferred to the anode resulting in current (r_a). It is of note that the model does not include several electron transfer steps from the inner membrane R_{ox}/$R_{\text{red}}H$ to periplasmic and outer membrane redox centers, but it simulates a direct electron transfer from R_{ox}/$R_{\text{red}}H$ to the biofilm matrix. Subfigures a) and b) were adapted from Korth and Harnisch, 2019, and Korth et al., 2015, respectively.

2. Material and methods

2.1 General remarks

All used chemicals were of technical grade or higher (VWR International, USA and Thermo Fisher Scientific Inc., USA). All mentioned potentials refer to the standard hydrogen electrode (SHE) by conversion from Ag/AgCl 3 M KCl reference electrode (+0.203 V vs. SHE).

2.2 Experimental setup and reactor configuration

Electroactive biofilms were chronoamperometrically cultivated on transparent fluorine-doped tin oxide (FTO) coated glass electrodes (Nippon Sheet Glass Co., Ltd., Japan), serving as anodes in a double-chambered flow cell. The reactor design has been previously described (Molenaar et al., 2018). Briefly, the anode compartment was composed of a flow channel (33 cm^3), and a graphite sheet (Voltea Inc., USA) was used as current collector for the FTO electrode. The flat and transparent electrode surface with an area of 22.3 cm^2 allowed the non-invasive biofilm monitoring via optical coherence tomography (OCT). A bipolar membrane (Ralex PEBPM, MEGA a.s., Czech Republic) was placed between the anode and cathode compartment to prevent crossover of, e.g., cathodically produced hydrogen to the anode. The cathode compartment was composed of a flow channel identical to the anode compartment with a flat platinum/iridium coated titanium plate (Pt/IrO2 80:20, Magneto special anodes B.V., The Netherlands) serving as cathode. In addition, a Ag/AgCl 3 M KCl reference electrode (Prosense B.V., The Netherlands) was used.

Each electrode chamber was connected to a feed and recirculation peristaltic pump (Masterflex L/S, Cole-Parmer®, Instrument Solutions Benelux B.V., The Netherlands). The feed was stored in a 10 L reservoir (Laboratory Glass Specialists B.V., The Netherlands) and pumped at 0.36 mL min^{-1}. The recirculation rate of anolyte and catholyte was 60 mL min^{-1}. Effluents from anodic and cathodic chambers were collected in 10 L reservoirs. Considering the total volume of the anolyte (220 mL, i.e., anode compartment and belonging tubing), 10 h hydraulic retention time (HRT) was obtained. A potentiostat (N-stat d-module, Ivium Technologies, The Netherlands) was used to apply a constant anode potential with current being sampled every minute. The reference electrodes were connected to the anode flow channel using a Haber-Luggin capillary (ProSense B.V., The Netherlands) filled with 3 M KCl solution and positioned at 5 mm distance to the FTO electrode. Quick-coupler valves (SS-QC4-D-400, Swagelok, USA) were connected to the tubing of each reactor to avoid oxygen penetration into the system, while reactors were disconnected for OCT analysis. The reactor temperature was controlled in a climate chamber at 298.15 K.

2.3 Inoculum and electrolyte composition

Reactors were inoculated with biomass collected from anodic electroactive biofilms fed with acetate. The microbial community was not directly determined, but we have excellent reasons to anticipate a high share of *Geobacter* species within the acetate-fed anodic electroactive biofilm. For instance, its enrichment using the here applied conditions was demonstrated several times (Commault et al., 2013; Korth et al., 2020b; Torres et al., 2009) even with the same experimental setup (Pereira et al., 2022a). Furthermore, the determined formal potential ($\Delta E^{\text{f}\prime}_{\text{Rox/RredH}}$ = −0.164 V) (Fricke et al., 2008) and the high Coulombic efficiency (90 ±24 %) (Commault et al., 2015;

Jung and Regan, 2007) indicate a typical *Geobacter* enrichment biofilm cultivated at anodes. Furthermore, 2-bromoethanesulfonic acid was added to the medium to inhibit methanogenesis. In addition, in a previous study with the same setup and comparable experimental conditions (E_A = −0.15 V, 10 mM acetate, *Geobacter* exhibited a relative abundance of ca. 75 % within the biofilm (Pereira et al., 2022a). Consequently, we focus on the genus *Geobacter* in the discussion of results, in line with the main body of literature on physiological adaptations to changing redox potentials of the TEA as well as the energetic consequences thereof. It is also of note that in the previous publication, only anaerobic bacteria were identified, and thus, we assume a biofilm consisting of almost only electroactive microorganisms performing acetate oxidation and EET to the anode, albeit the biofilm did not solely consist of *Geobacter* (Pereira et al., 2022a)

The anolyte constituted of (g L^{-1}): 3.40 KH_2PO_4, 4.36 K_2HPO_4, 0.1 $MgSO_4 \times 7H_2O$, 0.74 KCl, 0.58 NaCl, 0.28 NH_4Cl, 0.1 $CaCl_2 \times 2H_2O$, 1 mL of trace metals mixture, and 1 mL of vitamins mixture according to DSMZ culture medium 141 (Deutsche Sammlung von Mikroorganismen und Zellkulturen, Braunschweig, Germany). 0.04 (0.5 mM), 0.17 (2 mM), 0.41 (5 mM), or 0.65 (8 mM) $NaCH_3COO^-$ were added as electron donor. 1.97 g L^{-1} of $BrCH_2CH_2SO_3Na$ was added to the medium to inhibit methanogenesis. The anolyte inflow was continuously sparged with nitrogen during the experiments to maintain anaerobic conditions. The catholyte was a 50 mM potassium phosphate buffer solution at pH 7. Nitrogen was continuously sparged into the catholyte during reactor operation to avoid accumulation and crossover of hydrogen.

2.4 Experimental design

The range of acetate concentrations was chosen to include limiting (0.5 and 2 mM) and non-limiting (5 and 8 mM) acetate concentrations for electroactive biofilms (Kretzschmar et al., 2016). In addition, three different anode potentials (E_A, −0.2, −0.1, and 0 V) were applied. Every combinations of anode potential and acetate concentration were experimentally studied. Every condition was tested in duplicates so that 24 experiments were conducted in total (21 experiments were evaluable as three experiments did not result in biofilm growth). In these experiments, acetate concentration in influent and effluent, pH, and biomass production (via OCT) were measured every 2 to 3 days.

2.5 Acetate consumption and online monitoring of biofilm growth

Acetate consumption in the reactor was determined as the difference between the influent and effluent concentrations. After filtration through a 0.45 µm pore-size filter (EMD Millipore SLFH025NS, Merck KGaA, Germany), acetate concentration was measured using Ultra-High-Performance Liquid Chromatography (UHPLC, 300 × 7.8 mm Phenomenex Rezex Organic Acid H+ column, Dionex ultimate 3000RS, UV detector at a wavelength of 210 nm, Thermo Fisher Scientific, The Netherlands). The coefficient of determination R^2 for acetate quantification was 0.99996. The coulombic efficiency (*CE*) was calculated as ratio of the integrated current and the consumed acetate in a certain time interval.

After hydraulically and electrically disconnecting the reactors from the system, OCT was used to scan the FTO electrode at 54 evenly distributed spots. The resulting images were processed using a MATLAB script that isolated and counted the biofilm pixels. The number of pixels was converted to biomass weight [mgCOD] using the calibration reported by Molenaar et al. (Molenaar et al., 2018). For the subsequent calculations on biomass yields, only the duration until the first decrease in biomass weight (e.g., due to biofilm detachment) was considered, on average, 12 ±5 days.

2.6 Calculating the biomass yield of electroactive biofilms based on experimental data

2.6.1 Biomass yield based on acetate consumption ($Y_{X/ac}$)

The total acetate consumption (n_ac [mol]) of one experiment was calculated by summarizing the consumed acetate of all recorded time intervals (Δt [s]) according to equation 1.

$$n_\mathrm{ac} = \sum \left(C_\mathrm{ac,influent} - C_\mathrm{ac,effluent}\right) \times Q \times \Delta t \qquad (1)$$

$C_{\mathrm{ac,influent}}$ [mol L^{-1}] and $C_{\mathrm{ac,effluent}}$ are acetate concentration in the influent and effluent, respectively, Q is flow rate [L s^{-1}]. Subsequently, the biomass yield based on acetate consumption ($Y_{\mathrm{X/ac}}$ [mgCOD$_{\mathrm{biomass}}$ gCOD$_{\mathrm{ac}}^{-1}$]) was calculated using the biomass weight (COD_{biofilm} [mg]) obtained from OCT measurements and a COD conversion factor of 64 gCOD mol^{-1} for acetate (SI-1) (eq. 2).

$$Y_{\mathrm{X/ac}} = \frac{COD_{\mathrm{biofilm}}}{n_{\mathrm{ac}} \times 64\ \mathrm{gCOD\ mol^{-1}}} \tag{2}$$

2.6.2 Biomass yield based on catabolic energy harvest ($Y_{X/cat}$)

For determining $\mathrm{Y_{X/cat}}$, we followed the principles of a restricted energy harvest of EAM. Thus, the standard Gibbs energy of catabolic reaction ($\Delta_{\mathrm{R}}G_{\mathrm{cat}}^{0\prime}$ [kJ mol^{-1}]) was based on the direct coupling of acetate oxidation with the reduction of intracellular redox centers ($\mathrm{R_{ox}}$/$\mathrm{R_{red}H}$, eq. 3) located at the inner membrane using literature values for biochemical standard conditions (Heijnen and Kleerebezem, 2010). The Gibbs energy of formation of redox centers, required for the calculation of $\Delta_{\mathrm{R}}G_{\mathrm{cat}}^{0\prime}$, was calculated using the formal redox potential ($E_{\mathrm{Rox/RredH}}^{\mathrm{f}\prime}$, SI-2) obtained from cyclic voltammetry (CV) experiments (SI-3, see discussion in section 3.3). The determined $E_{\mathrm{Rox/RredH}}^{\mathrm{f}\prime}$ = −0.164 ±0.009 V is indicative for a *Geobacter* dominated biofilm (Fricke et al., 2008). It is necessary to mention that using CV data as input parameter for inner membrane cytochromes represents an approximation as formal potentials derived from turnover CV represent mixed potentials that are not determined by only one reaction, but influenced by different cytochromes and their redox states under particular growth conditions. Information on the localization of specific cytochromes can be, for instance, obtained by open circuit potential measurements (Schrott et al., 2019). However, the determined $E_{\mathrm{Rox/RredH}}^{\mathrm{f}\prime}$ is close to formal potentials of inner membrane cytochromes of *Geobacter sulfurreducens* (e.g., CbcL, E^{f} = −0.150 V) (Reguera and Kashefi, 2019; Zacharoff et al., 2016). For the calculations, redox centers were assumed to be one-electron carriers performing proton-coupled electron transfer (i.e., redox-Bohr effect (Morgado et al., 2012)).

$$\mathrm{C_2H_3O_2^- + 4H_2O + 8R_{ox} \rightarrow 2HCO_3^- + 8R_{red}H + H^+} \qquad \Delta_{\mathrm{R}}G_{\mathrm{cat}}^{0\prime} = -88.3\,\frac{\mathrm{kJ}}{\mathrm{mol}} \tag{3}$$

Subsequently, $\Delta_{\mathrm{R}}G_{\mathrm{cat}}^{0\prime}$ was corrected for actual experimental conditions using eq. 4 and experimental data for pH and acetate.

$$\Delta_{\mathrm{R}}G_{\mathrm{cat}} = \Delta_{\mathrm{R}}G_{\mathrm{cat}}^{0\prime} + RT \times \ln\left[\left(\frac{C_{\mathrm{HCO3-}}}{1\ \mathrm{mol\ L^{-1}}}\right)^2 \left(\frac{C_{\mathrm{H+}}}{10^{-7}\ \mathrm{mol\ L^{-1}}}\right)\left(\frac{1\ \mathrm{mol\ L^{-1}}}{C_{\mathrm{ac,effluent}}}\right)\left(\frac{C_{\mathrm{RredH}}}{C_{\mathrm{Rox}}}\right)^8\right] \tag{4}$$

$\Delta_{\mathrm{R}}G_{\mathrm{cat}}$ [kJ mol^{-1}] is Gibbs energy of catabolic reaction corrected for experimental conditions, R is the universal gas constant (8.314 J K^{-1} mol^{-1}), T [K] is temperature, C_{i} is concentration of *i*-th species. For simplicity, it was assumed that the acetate concentration within the biofilm and in the medium (i.e., $C_{\mathrm{ac,effluent}}$) are equal. $C_{\mathrm{HCO3-}}$ was calculated considering consumed acetate (eq. 5) and the ratio $\frac{\mathrm{R_{red}H}}{\mathrm{R_{ox}}}$ was based on UV/Vis spectroscopy of *Geobacter sulfurreducens* biofilms (Liu and Bond, 2012), considering the applied anode potential and biofilm thickness (SI-4).

$$C_{\mathrm{HCO3-}} = 2 \times (C_{\mathrm{ac,influent}} - C_{\mathrm{ac,effluent}}) \tag{5}$$

Assuming a constant acetate oxidation rate during sample intervals, the total microbial energy harvest (U [kJ]) was obtained according to eq. 6. U describes the energy harvested from all catabolic reactions in the biofilm(Korth and Harnisch, 2019). Subsequently, this energy is utilized for biomass growth, maintenance, and energy dissipation.

$$U = \Delta_{\mathrm{R}}G_{\mathrm{cat}} \times n_{\mathrm{ac}} \tag{6}$$

Finally, the biomass yield based on catabolic energy harvest ($Y_{\mathrm{X/cat}}$ [mgCOD$_{\mathrm{biomass}}$ kJ^{-1}]) was calculated according to eq. 7.

$$Y_{\mathrm{X/cat}} = \frac{COD_{\mathrm{biofilm}}}{U} \tag{7}$$

2.7 Calculating the biomass yield of electroactive biofilms based on thermodynamic modeling

2.7.1 Model description

A previously developed non-equilibrium thermodynamic model for electroactive biofilms (Korth et al., 2015) was refined and applied to compare experimental and modeled biomass yields. In brief, the model simulates processes like biofilm growth, diffusion, migration, and electron transport within the biofilm by combining biological, chemical, physicochemical, and electrochemical equations at different system levels, including microbial cell, biofilm, and reactor. The model refinement presented in this study comprises an adjusted incorporation of the restricted energy harvest of electroactive microorganisms (in the original model, only the energy difference between acetate and NAD$^+$/NADH was considered as microbial energy harvest), pH dependency of redox centers, continuous conditions, and bidirectional ion transport across the membrane (SI-5).

The microbial cells utilize acetate for harvesting energy leading to current production (i.e., catabolic reaction) and for biomass formation (i.e., anabolic reaction). Reduced reduction equivalents (i.e., NADH) produced during acetate oxidation are intracellularly oxidized so that the electrons are transferred to redox centers located at the inner membrane (R_{ox}/$R_{red}H$) and further to the extracellular biofilm matrix, which collects all electrons from all biofilm cells transferring the electrons finally to the anode (Fig 1b). Being in line with time-resolved surface-enhanced resonance Raman spectroscopy data, by Ly et al. (Ly et al., 2013), the model distinguishes between homogeneous (between inner membrane redox centers and extracellular biofilm matrix) and heterogeneous (between biofilm matrix and anode) electron transfer both modeled with the Butler-Volmer equation but with different rate constants (SI-5). Only the acetate oxidation and the electron transfer from NADH to R_{ox} contribute to the energy harvest but not the homogeneous and heterogeneous electron transfer as they discretely simulate the electron transfer from the inner membrane across periplasm, outer membrane, and biofilm matrix to the anode. A variety of literature data was used as input parameters for the model, and the model output was validated with literature data to increase its significance. A complete model description can be found in Korth et al., 2015. For this study, the model was tailored to consider the design (e.g., reactor and electrode size, flow rate, medium composition, and anode potential) of the experimental study (see SI-5 for main model parameters and adapted equations). For creating the model and for performing simulations, COMSOL Multiphysics V5.1 (COMSOL Inc., Sweden) was used.

2.7.2 Biomass yield based on catabolic energy harvest ($Y_{X/cat}$)

The catabolic reaction was modified to consider the restricted energy harvest of EAM adequately. In detail, acetate oxidation was coupled to NAD$^+$ reduction (eq. 8), and biological energy transduction at the electron transport chain (i.e., conversion of reduction equivalents in ATP) was simulated by coupling NADH oxidation to the reduction of inner membrane redox centers (e.g., inner membrane cytochromes, eq. 9). Both corresponding Gibbs energies ($\Delta_{\mathrm{R}}G^{0\prime}_{\mathrm{cat1}}$ and $\Delta_{\mathrm{R}}G^{0\prime}_{\mathrm{cat2}}$) were corrected for actual experimental conditions following eq. 4 (SI-6) in order to obtain ΔG_{cat1} and ΔG_{cat2}.

$$\mathrm{C_2H_3O_2^- + 4H_2O + 4NAD^+ \rightarrow 2HCO_3^- + 4NADH + 5H^+} \qquad \Delta_{\mathrm{R}}G^{0\prime}_{\mathrm{cat1}} = 32.3\,\frac{\mathrm{kJ}}{\mathrm{mol}} \tag{8}$$

$$\mathrm{NADH + 2R_{ox} + H^+ \rightarrow 2R_{red}H + NAD^+} \qquad \Delta_{\mathrm{R}}G^{0\prime}_{\mathrm{cat2}} = -30.2\,\frac{\mathrm{kJ}}{\mathrm{mol}} \tag{9}$$

In accordance with section 2.6.2, redox centers were assumed to be one-electron carriers. Their difference in Gibbs energy of formation was based on CV results as already described in section 2.6.2 (see also SI-2). The difference in

Gibbs energy of formation of the redox couple NAD$^+$/NADH was similarly obtained as previously explained (Korth et al., 2015).

The Gibbs energies of both catabolic reactions were integrated over biofilm thickness and time, considering all catabolic reactions within the biofilm during the whole simulation time (t) for obtaining the total microbial energy harvest (eq. 10).

$$U = \left[\int_0^t \left(\int_0^x \Delta G_{\mathrm{cat1}} r_{\mathrm{ac,cat}} \mathrm{d}x \right) \mathrm{d}t + \int_0^t \left(\int_0^x \Delta G_{\mathrm{cat2}} r_{\mathrm{i}} \mathrm{d}x \right) \mathrm{d}t \right] \times A_{\mathrm{anode}} \tag{10}$$

$r_{\mathrm{ac,cat}}$ [mol s^{-1} L^{-1}] is catabolic acetate consumption rate (only considering acetate consumption for energy harvesting but not for anabolism) based on a double Michaelis-Menten kinetics (i.e., considering availability of acetate and NAD$^+$), x [µm] is biofilm thickness, r_{i} [mol s^{-1} L^{-1}] is intracellular electron transfer rate between NAD$^+$/NADH and R_{ox}/R_{red}H (this reaction rate is based on the concentrations of the reactants and rate constants of forward and backward reaction) (Korth et al., 2015), and A_{anode} [cm^2] is anode area. After normalizing the produced biomass to COD equivalents (eq. 11, SI-7) to allow a direct comparison with OCT experiments, the modeled biomass yield based on the microbial energy harvest was calculated according to eq. 12.

$$COD_{\mathrm{biofilm}} = x \times A_{\mathrm{anode}} \times C_{\mathrm{X}} \times 44.8 \text{ gCOD C-mol}^{-1} \tag{11}$$

$$Y_{\mathrm{X/cat}} = \frac{COD_{\mathrm{biofilm}}}{U} \tag{12}$$

C_{X} [2000 C-mol m^{-3}] is biomass density (Korth et al., 2015).

2.7.3 Biomass yield based on acetate consumption ($Y_{X/ac}$)

Total acetate consumption (n_{ac}) was calculated by integrating the acetate consumption rate over biofilm thickness and time (eq. 13). Subsequently, the modeled biomass yield based on acetate consumption was calculated (eq. 14).

$$n_{\mathrm{ac}} = \int_0^t \left(\int_0^x r_{\mathrm{ac}} \mathrm{d}x \right) \mathrm{d}t \times A_{\mathrm{anode}} \tag{13}$$

$$Y_{\mathrm{X/ac}} = \frac{COD_{\mathrm{biofilm}}}{n_{\mathrm{ac}} \times 64 \text{ gCOD mol}^{-1}} \tag{14}$$

2.8 Statistics

Results are presented as means with the corresponding confidence interval (α = 0.05).

3. Results and Discussion

3.1 Electrochemical characterization of electroactive biofilms

For all experimental conditions, biofilm growth and current production were monitored over time. Figure 2 illustrates two examples of the development of current density (j) and biomass for limiting (i.e., low acetate concentration, $C_{\mathrm{ac,influent}}$ = 0.5 mM, and low anode potential, E_{A} = –0.2 V) and non-limiting (i.e., $C_{\mathrm{ac,influent}}$ = 5 mM and E_{A} = 0 V) conditions. In all cases, j rapidly increased in the beginning without an apparent lag phase (SI-8). Within a few days, j saturated and remained constant for non-limiting conditions. When limiting conditions were applied, j usually decreased after reaching its maximum and stabilized at a lower value.

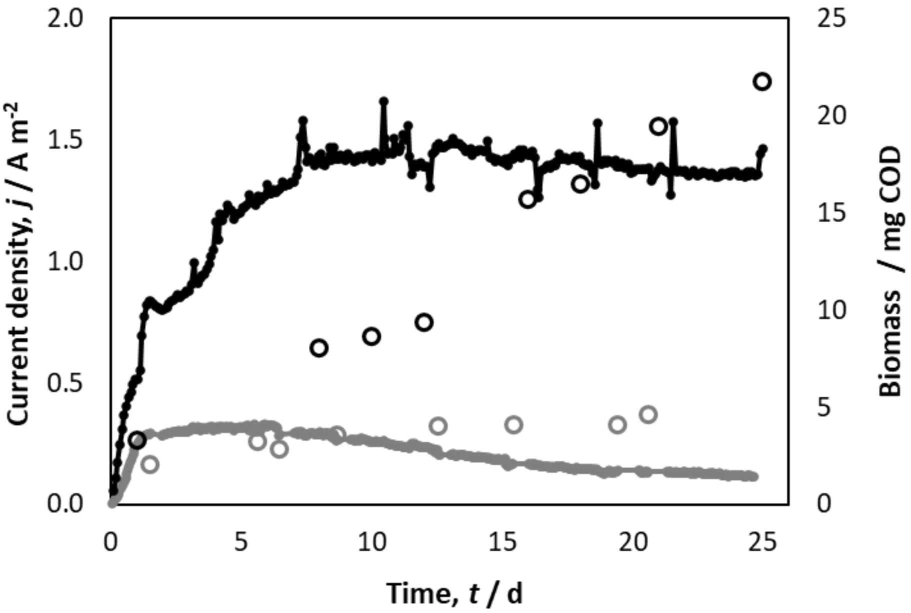

Figure 2 Time course of exemplary experiments showing current densities (lines) and corresponding biomass growth (circles). Experiments were performed with an acetate concentration of 0.5 mM at −0.2 V (grey, limiting conditions) and 5 mM at 0 V (black, non-limiting conditions).

Current densities did not exceed 0.3 A m^{-2} when $C_{\mathrm{ac,influent}}$ was 0.5 mM. For this low substrate concentration, changes in anode potential did not have any effect on j, representing acetate-limited conditions. For $C_{\mathrm{ac,influent}}$ of 2 mM and 5 mM, j ranged from 0.5 to 2.5 A m^{-2}, while 8 mM resulted in a higher current density of 1.3 to 3.5 A m^{-2}. For all acetate concentrations, the highest j were measured at −0.1 V and 0 V with only minor differences between them. For instance, in case of 8 mM acetate, a steep current increase was observed when the anode potential was changed from −0.2 V to −0.1 V, but a further increase to 0 V led to a less evident rise of current, indicating limiting and non-limiting potential conditions for −0.2 V and 0 V, respectively.

For all tested anode potentials and acetate concentrations, biomass growth was observed via OCT at the beginning of the experiments, while current production was negligible. Consequently, coulombic efficiency (*CE*) was low at the beginning of most experiments but reached 90 ±24 % when complete experiments were considered. This indicates that a considerable share of acetate (and thus electrons) were directed toward biomass formation in the early growth phase, as it was already demonstrated for batch cultures with anodic *Geobacter* enrichment biofilms (Korth et al., 2020a). After substantial biomass was formed, biofilm growth slowed, and more acetate was channeled through catabolism leading to an increasing *CE* during experiments. Intriguingly, the model showed a similar behavior during all simulations with comparable low *CE* initially, subsequently increasing and leveling off at around 95 %.

3.2 Biomass yields of electroactive biofilms

By averaging all experimental results, a biomass yield based on acetate consumption ($Y_{\mathrm{X/ac}}$) of 36.7 ±8.6 $\mathrm{mgCOD_{biomass}\ gCOD_{ac}^{-1}}$ (or expressed in dry weight 30.9 ±7.3 $\mathrm{mgDW_{biomass}\ g_{ac}^{-1}}$, Table 1) was derived. This is in line with previously published growth yields of 38-42 $\mathrm{mgCOD_{biomass}\ gCOD_{ac}^{-1}}$ obtained with a similar experimental design used for establishing OCT as method for *in situ* biomass quantification of electroactive biofilms (Molenaar et al., 2018). Similar to this previous work, calculations on biomass yield were solely based on biofilm growth and did not consider the proliferation of planktonic cells and their wash-out in the continuous system. However, due to the absence or negligible concentration (sulfate) of alternative soluble terminal electron acceptors and the use of 2-bromoethanesulfonic acid to inhibit methanogenesis, it is unlikely that a substantial fraction of acetate was directed to the formation of a planktonic phase. Biofilm detachment could also have contributed to the occurrence of planktonic cells. However, as biofilm detachment infers with biofilm quantification via OCT, only the experimental duration before biofilm decrease being observed was considered for all calculations. Generally, $Y_{\mathrm{X/ac}}$ showed the opposite behavior compared to *CE*, as it was initially high but decreased within a few days and leveled off during the experiment. However, for improved time-resolved analysis of the biomass yield, more replicates are required, and cultivation of pure cultures could reduce the observed experimental variability. This investigation would also include the application of more positive anode potentials to prove the hypothesized generality of the observed results. When the experimentally obtained data is normalized to molarities, it can be seen that the biomass yield of acetate-fed electroactive biofilms (0.074 $\text{C-mol}_{\text{biomass}}\ \text{C-mol}_{\text{substrate}}^{-1}$) is in the lower range compared to biomass yields reported for several other anaerobes growing on different carbon sources including fermentative microorganisms and methanogens (Heijnen and van Dijken, 1992). This observation verifies the calculations for the standard Gibbs energy of catabolic reaction of the electroactive biofilm ($\Delta_{\mathrm{R}}G^{0\prime}_{\mathrm{cat}}$ = −88.4 kJ mol^{-1}, Eq. 3) as $\Delta_{\mathrm{R}}G^{0\prime}_{\mathrm{cat}}$ is in the same range as, for instance, hydrogenotrophic (−135.5 kJ mol^{-1}) and acetoclastic (−31.0 kJ mol^{-1}) methanogenesis, acetogenesis (−104.5 kJ mol^{-1}) (SI-9), fermentation of butanediol to acetate and ethanol (−38.2 kJ mol^{-1}), or fermentation of acetoin to acetate and ethanol (−75.4 kJ mol^{-1}) (Schink, 1984).

The biomass yield can also be normalized to the catabolic energy harvest ($Y_{\mathrm{X/cat}}$) using time-resolved experimental data (sections 2.6.2 and 2.7.2). By doing so, biomass yield is related to all energy-yielding reactions occurring within the biofilm. Taking all experiments into account, $Y_{\mathrm{X/cat}}$ amounts to 25.9 ±6.8 $\text{mgCOD}_{\text{biomass}}\ \text{kJ}^{-1}$ (or expressed in dry weight 21.8 ±5.7 $\text{mgDW}_{\text{biomass}}\ \text{kJ}^{-1}$, Table 1). This value is beneficial for establishing holistic energy balances of MET in future as it facilitates the incorporation of microbial energy demand together with other processes that produce or consume chemical, electrical, or heat energy. Consequently, comprehensive economic assessments of MET and direct comparisons with other (bio)technological approaches (Kontogeorgis and Folas, 2010; von Stockar and von der Wielen, 2003) are feasible.

Table 1 Overview of the biomass yields obtained experimentally by OCT measurements and by thermodynamic modeling

	Units[a]	Experiments	Thermodynamic modeling
Biomass yield based on acetate consumption, $Y_{\mathrm{X/ac}}$	$\text{mgCOD}_{\text{biomass}}\ \text{gCOD}_{\text{ac}}^{-1}$	36.7 ±8.6	23.8 ±3.9
	$\text{mgDW}_{\text{biomass}}\ \text{g}_{\text{ac}}^{-1}$	30.9 ±7.3	20.0 ±3.1
Biomass yield based on catabolic energy harvest, $Y_{\mathrm{X/cat}}$	$\text{mgCOD}_{\text{biomass}}\ \text{kJ}^{-1}$	25.9 ±6.8	35.6 ±4.8
	$\text{mgDW}_{\text{biomass}}\ \text{kJ}^{-1}$	21.8 ±5.7	30.0 ±4.1

[a] 0.78 $\text{mgDW}_{\text{biomass}}\ \text{mgCOD}_{\text{biomass}}^{-1}$ and 1.08 $\text{gCOD}_{\text{ac}}\ \text{g}_{\text{ac}}^{-1}$ were used as conversion factors. For more details, please see SI-10.

3.3 Comparison of biomass yields obtained by experiments and thermodynamic modeling

To obtain further knowledge on the energy metabolism of EAM, the experimental data was compared to results obtained with the enhanced thermodynamic model on EAM (section 2.7.1 and Korth et al., 2015). All conducted experiments were simulated in order to compare modeled and experimentally derived biomass yields using total charge production as optimization parameter. Intriguingly, only one model parameter (i.e., the rate constant for the heterogeneous electron transfer from the biofilm matrix to the anode, k_{a}^{0} = 0.032 ±0.028 s^{-1}, *n* = 21) had to be slightly adjusted to simulate charge production (deviation 0.5 ±1.3 %) of experiments within the same time interval. Presumably, material and geometric inhomogeneities of the used FTO electrodes led to different charge transfer resistances requiring adaptions of k_{a}^{0} for the different simulations. Although the applied values for k_{a}^{0} indicate a (quasi-)reversible electron transfer; the applied anode potential (−0.2 V to 0 V vs. SHE) is in the potential range where EET may limit the catabolism (see SI-3, cyclic voltammograms).

Interestingly, the modeled $Y_{\mathrm{X/ac}}$ and $Y_{\mathrm{X/cat}}$ exhibited opposite tendencies when they were compared with their experimental counterparts. Whereas $Y_{\mathrm{X/ac}}$ derived from modeling was ca. 35 % lower compared to the experimental value, the modeled $Y_{\mathrm{X/cat}}$ was ca. 30 % higher than the biomass yield obtained from experiments (Table 1).These observed yield differences have several implications for the thermodynamic modeling of electroactive biofilms considering the average modeled catabolic energy harvest of −40.9 ±2.8 kJ $\mathrm{mol_{ac}}^{-1}$ (SI-11). This value translates to an upper thermodynamic limit of 0.7 $\mathrm{mol_{ATP}}$ $\mathrm{mol_{ac}}^{-1}$ assuming an energy requirement of −60 kJ mol^{-1} for ATP synthesis at physiological conditions (Nelson and Cox, 2017) being in line with the theoretical maximum yield of 0.5 $\mathrm{mol_{ATP}}$ $\mathrm{mol_{ac}}^{-1}$ proposed by Mahadevan *et al*. for *G. sulfurreducens* using soluble Fe(III) citrate as TEA which also leads to a restricted energy harvest (Mahadevan et al., 2006). Therefore, we propose that the "energy input" (i.e., the restricted catabolic energy harvest of EAM only exploiting the energy difference between the substrate and the electron-transport chain) was adequately modeled. However, it seems that the energy utilization (i.e., mainly growth and maintenance) requires refinements for improved simulations.

The underestimation of $Y_{\mathrm{X/ac}}$ by the model indicates that processes that directly influence the biomass yield (e.g., maintenance requirements and amount of dissipation energy needed to facilitate growth) are overestimated. Thus the available energy for biomass growth is underestimated. To calculate microbial growth parameters, the model applied a well-established method based on Gibbs energy of dissipation which results are consistent compared to the efficiency of energy capture approach (Heijnen and Kleerebezem, 2010; VanBriesen, 2002). Nevertheless, applying these methods to anaerobic growth systems is still a delicate endeavor leading to significant uncertainties (Liu et al., 2007). Moreover, the maintenance requirements are indeed based on large data collection of aerobic and anaerobic microorganisms, but biofilm cultures were not included in this analysis. Biofilms and planktonic cells usually exhibit certain physiological differences as cellular functions like stress response and motility are less required within the biofilm than in planktonic cells (Dumitrache et al., 2017). It was also shown for the anaerobic bacteria *Clostridium thermocellum* that genes for the energy metabolism are differently expressed in biofilm and planktonic state (Dumitrache et al., 2017). Therefore, a customized growth model for electroactive biofilms is required, considering the particular properties of EAM and biofilm physiology. To our knowledge, experimental data on maintenance requirements is only available for the planktonic growth of the model organism *G. sulfurreducens* using fumarate and Fe(III) citrate as TEA (Mahadevan et al., 2006). However, a generalized growth model has to be based on different EAM consuming different substrates and using soluble as well as solid TEA. Another potential reason for the observed deviations of the yield could be the biomass composition. In the model, a conventional formula for biomass was used ($CH_{1.8}O_{0.5}N_{0.2}$, (Roels, 1980)), but recent results indicate that the elemental composition of *G. sulfurreducens* biofilms is more reduced compared to microorganisms breathing soluble electron acceptors (Howley et al., 2022) resulting in different energy demands for anabolic processes.

The overestimation of $Y_{\mathrm{X/cat}}$ by thermodynamic modeling clearly suggests that the assumption of the restricted catabolic energy harvest is correct. Moreover, a comparison of modeling and experimental results indicates that the catabolic energy harvest is even more restricted than delineated by model assumptions or that further processes occur that decrease the availability of the harvested catabolic energy. For instance, the microbial electrochemical Peltier heat (mePh) constitutes an entropic barrier at the interface EAM/anode that requires an energy investment to be overcome (Korth et al., 2016). At the same, the mePh represents an entropic contribution to the driving force for growth. So far, only the mePh of *Geobacter* enrichment biofilms transferring electrons to a graphite electrode was measured (27 ±6 kJ mol^{-1}) (Korth et al., 2016). Still, it is supposed to vary depending on the active redox species (e.g., outer membrane cytochromes of EAM), the electrode material, and the electrolyte considering its abiotic equivalent, the electrochemical Peltier heat (Fang, 2011).

3.4 (In-)Dependence of biomass yield from anode potential and acetate concentration

Generally, neither $Y_{\mathrm{X/ac}}$ nor $Y_{\mathrm{X/cat}}$ obtained from experiments and modeling showed clear correlations with acetate concentration or anode potential. Especially the comparable high variability of some experimental conditions resulted in a limited statistical significance of the results so that only a few trends for the thermodynamic model can be anticipated. For instance, a minor dependency of the modeled $Y_{\mathrm{X/ac}}$ and $Y_{\mathrm{X/cat}}$ on acetate concentration was indicated for anode potentials of 0 V and −0.1 V, but only with low coefficients of determination (SI-12). For E_{A} = −0.2 V, the model predicts no dependence of biomass yield from acetate concentration, indicating that the TEA limitation governs microbial activity. Also, the model indicated no clear dependence of the biomass yield on anode potential. At C_{ac} of 5 mM and 8 mM, the biomass yield weakly increases with more positive anode potentials. Surprisingly, the opposite was observed for C_{ac} = 2 mM (SI-12). This could be explained by the complex interplay of different partially opposite gradients and kinetics within the electroactive biofilm (see discussion below), leading to the occurrence of an energetic minimum of the thermodynamic frame (i.e., maximum available energy that catabolic reactions can harvest) (Korth and Harnisch, 2019).

The experimental independence of the acetate concentration on biomass yield was unexpected, as it is in strong contrast to planktonic cultures of *G. sulfurreducens* cultivated at limited and excessive availability of ED or TEA (Esteve-Núñez et al., 2005). Besides the experimental comparable high variability, other reasons could had contributed as well. For instance, gradients within the biofilm, the small sample size for similar experimental conditions not capturing the biological variance of electroactive biofilms (Larrosa et al., 2009), the inherent challenges for a reliable determination of biomass yields (Liu et al., 2007), and the physiological differences between biofilm and planktonic cells (Berlanga and Guerrero, 2016). Electroactive biofilms are complex systems with several internal gradients (substrate, pH, counter ion, and redox potential) (Atci et al., 2016; Babauta et al., 2012; Franks et al., 2009; Pereira et al., 2022b). Conceivably, this leads to different activities and hence biomass yields in different biofilm layers, depending on biofilm thickness and density. Similarly, these gradients could also conceal a putative relation between biomass yield and anode potential that relies on the synthesis of different inner membrane cytochromes in response to the available TEA, as demonstrated for *G. sulfurreducens* (Joshi et al., 2021; Levar et al., 2014; Zacharoff et al., 2016). With this mechanism, *G. sulfurreducens* can presumably maximize its total microbial energy harvest (i.e., U) as more positive TEA lead to the production of inner membrane cytochromes with higher redox potentials. Consequently, lower anode potentials lead to the expression of inner membrane cytochromes with low redox potentials, which decreases the maximum available energy (i.e., U) as the energy difference between the electron donor and the inner membrane cytochrome decreases. Nevertheless, this mechanism ensures that EET can still proceed at a sufficient rate as the energy difference between inner membrane cytochromes and the cytochrome network in the periplasm and at the outer membrane and, thus, the anode remains exergonic. For *G. sulfurreducens,* it is described that for anode potentials more positive than −0.1 V, mainly the inner membrane cytochrome ImcH is active whereas below −0.1 V, CbcL is dominating (Levar et al., 2014). Although a more negative a more positive anode potential than -0.1V is applied in this study, no changes in biomass yield were observed likely due to the abovementioned superimposed gradients within the biofilm.

The applied thermodynamic model not consider the effects of changes within the electron transport chain or the influence of the anode material on the overall energy balance due to the lack of sufficient experimental data that could be used as input parameters (e.g., cytochrome concentrations, electron transfer rate constants). Yet, the implementation of different EET pathways is undoubtedly a future improvement of the model to further increase its significance

As mentioned above, the applied anode potential range is relatively narrow, eventually not triggering the synthesis of different inner membrane cytochromes. Yet, the range is of high practical relevance, as a low anode potential usually leads to higher power output in MFC (i.e., converting chemical energy stored in wastewater into electrical energy) or lower required energy input and higher overall energy efficiency in microbial electrolysis cells (MEC, i.e., converting chemical energy stored in wastewater with electricity input into hydrogen).

3.5 Biotechnological implications

The obtained results on biomass yields can be used to optimize biotechnological applications based on anodic electroactive biofilms energetically. Together with substrate uptake rates (Korth et al., 2020a; Kubannek et al., 2022) and an optimized anode potential (i.e., minimizing energy input for applying a potential but providing sufficient driving force for growth of EAM), a tailor-made feeding strategy for EAM could be designed optimizing biomass production. After EAM established sufficient biomass for a particular MET process, the anode potential (or the external resistance of a MFC) can be modulated for steering the energy fluxes towards improved energy efficiency of MET by decreasing the energy flux to the biomass. By doing so, further biomass formation would be minimized, and the probability of process failures (e.g., by biofilm detachment or by clogging of 3D electrodes due to the accumulation of inactive biomass) could be decreased.

In the following, we demonstrate how the obtained data on biomass yields can be used to estimate the impact of the energy needs of biofilm formation on the overall energy balance and thus on the economic feasibility of MFC (see SI-13 for detailed calculations). In a prototype study by Hiegemann et al., a submergible MFC module was presented, which can be integrated into existing wastewater treatment plants (WWTP) (Hiegemann et al., 2019). This module has an anode size of 4.2 m^2 and covers an area of 0.3 m^2. When taking the example of a rather small WWTP (55,000 population equivalents) with a daily wastewater inflow of 8050 m^3 and an average organic load of 0.4 $kgCOD\ m^{-3}$ (Korth et al., 2021), the primary clarifier (ca. 30×10 m) could host a maximum of 1000 MFC modules. For the formation of electroactive biofilms covering the total anode area of these 1000 MFC modules, a substrate input of 630 kgCOD would be required considering an average biofilm coverage of 5.5 $gCOD_{biomass}\ m^{-2}$ and a biomass yield of 36.7 $mgCOD_{biomass}\ gCOD^{-1}$, as both determined in this study. Therefore, only 0.05 % of the annual WWTP's total COD inflow is consumed for forming the electroactive biofilm, leaving the major part of the chemical energy within the wastewater for harvesting electric energy. Besides the proposed trade-off between power production and COD removal depending on the reactor configuration (Rossi and Logan, 2022), these calculations disclose one current major drawback of the MFC technology. Even with this vast anode area (4200 m^2), only ca. 2 % of the wastewater could be treated with the implemented MFC modules calling for reinforced engineering of reactor and anode geometries to achieve an optimized anode area-to-volume ratio while preventing limited mass transfer due to formation of excess biomass (Chong et al., 2019; Moß et al., 2019). Theoretically compensating for this insufficient treatment capacity in order to treat 100 % of the wastewater inflow with MFC modules, still only 3.8 % of the annual total chemical energy stored in wastewater would be required for biomass formation. Obviously, this examination represents only a first step towards an operational energy balance of MFC, but it underlines the energetic potential of MFC as well as its current bottlenecks for applications. It is common sense that in wastewater treatment plants also other biomass growth than anodic biofilms occurs as alternative electron acceptors (mainly oxygen but also, e.g., nitrate) are freely available, likely presenting a larger energy sink than the formation of anodic biofilms. Still, a CE of 10-30 % seems conceivable for a real-world application of MFC (Alsayed et al., 2020).

4. Conclusions

We investigated the biomass yield of acetate-fed electroactive biofilms and its dependency on acetate concentration and anode potential by applying optical coherence tomography. Furthermore, thermodynamic calculations and modeling were conducted to shed further light on the energy metabolism of EAM. The experimental biomass yield based on acetate consumption amounted to 36.7 ±8.6 $mgCOD_{biomass}\ gCOD_{ac}^{-1}$ and no clear trend between biomass yield and acetate concentration or anode potential were observed, calling for further investigations to improve the statistical significance. The ratio of biomass yield and catabolic energy harvest is well in line with literature about different anaerobic microorganisms verifying the applied thermodynamic model and calculation framework. Yet, at the same time, it demonstrates the complexity of electroactive biofilms exhibiting several internal gradients (e.g., redox potential, pH, and substrate), resulting in different growth efficiencies within different biofilm layers challenging the determination of general yield coefficients. A previously developed thermodynamic model for EAM was refined to allow adequate simulation of the restricted energy harvest of EAM and tailored to simulate the performed experiments. Thus, the general applicability of the thermodynamic model to simulate different experimental designs and concepts was demonstrated as only minor changes within the system of equations were required therefore. Experimentally derived and modeled biomass yields exhibited noticeable deviations indicating that the applied growth model requires adaptations for an improved description of the energy metabolism of electroactive biofilms. Especially considering the physiological differences between biofilm and planktonic state, the requirement for specified microbial maintenance and energy dissipation of electroactive biofilms seems evident. Furthermore, unique phenomena of EAM, like the microbial electrochemical Peltier heat, coincidently representing an entropic energy sink and a significant contribution to the driving force for growth, need to be considered in thermodynamic calculations. These refinements must be based on sets of experiments with a wide variety of different EAM consuming different substrates and TEA. Nevertheless, the obtained biomass yields can already be used to estimate the impact of biological energy demands in holistic energy balances of microbial fuel cells and other MET, contributing to assessments of their economic feasibility. Doing so showed that only a minor fraction of the chemical energy stored in wastewater is needed for sufficient biofilm formation covering the complete anode area to treat the daily wastewater inflow.

5. Acknowledgements

This work was supported by the Helmholtz Association in the frame of the Integration Platform “Tapping nature’s potential for sustainable production and a healthy environment” at the UFZ. This work is also part of the project “Understanding and controlling electron flows in electroactive biofilms” with project number 17516 of the research programme Vidi which is (partly) financed by the Dutch Research Council (NWO).

6. References

Alsayed, A., Soliman, M., Eldyasti, A., 2020. Microbial fuel cells for municipal wastewater treatment : From technology fundamentals to full-scale development. Renew. Sustain. Energy Rev. 134, 110367. https://doi.org/10.1016/j.rser.2020.110367

Atci, E., Babauta, J.T., Sultana, S.T., Beyenal, H., 2016. Microbiosensor for the detection of acetate in electrode-respiring biofilms. Biosens. Bioelectron. 81, 517–523. https://doi.org/10.1016/j.bios.2016.03.027

Babauta, J.T., Nguyen, H.D., Harrington, T.D., Renslow, R., Beyenal, H., 2012. pH, redox potential and local biofilm potential microenvironments within Geobacter sulfurreducens biofilms and their roles in electron transfer. Biotechnol. Bioeng. 109, 2651–62. https://doi.org/10.1002/bit.24538

Berlanga, M., Guerrero, R., 2016. Living together in biofilms: The microbial cell factory and its biotechnological implications. Microb. Cell Fact. 15, 1–11. https://doi.org/10.1186/s12934-016-0569-5

Bird, L.J., Bonnefoy, V., Newman, D.K., 2011. Bioenergetic challenges of microbial iron metabolisms. Trends Microbiol. 19, 330–340. https://doi.org/10.1016/j.tim.2011.05.001

Cao, X., Huang, X., Liang, P., Xiao, K., Zhou, Y., Zhang, X., Logan, B.E., 2009. A new method for water desalination using microbial desalination cells. Environ. Sci. Technol. 43, 7148–7152. https://doi.org/10.1021/es901950j

Chong, P., Erable, B., Bergel, A., 2019. Effect of pore size on the current produced by 3-dimensional porous microbial anodes: A critical review. Bioresour. Technol. 289, 121641. https://doi.org/10.1016/j.biortech.2019.121641

Commault, A.S., Lear, G., Packer, M.A., Weld, R.J., 2013. Influence of anode potentials on selection of Geobacter strains in microbial electrolysis cells. Bioresour. Technol. 139, 226–234. https://doi.org/10.1016/j.biortech.2013.04.047

Commault, A.S., Lear, G., Weld, R.J., 2015. Maintenance of Geobacter-dominated biofilms in microbial fuel cells treating synthetic wastewater. Bioelectrochemistry 106, 150–158. https://doi.org/10.1016/j.bioelechem.2015.04.011

Dou, W., Xu, D., Gu, T., 2021. Biocorrosion caused by microbial biofilms is ubiquitous around us. Microb. Biotechnol. 14, 803–805. https://doi.org/10.1111/1751-7915.13690

Dumitrache, A., Klingeman, D.M., Natzke, J., Rodriguez, M., Giannone, R.J., Hettich, R.L., Davison, B.H., Brown, S.D., 2017. Specialized activities and expression differences for Clostridium thermocellum biofilm and planktonic cells. Sci. Rep. 7, 1–14. https://doi.org/10.1038/srep43583

Esteve-Núñez, A., Rothermich, M., Sharma, M., Lovley, D.R., 2005. Growth of Geobacter sulfurreducens under nutrient-limiting conditions in continuous culture. Environ. Microbiol. 7, 641–648. https://doi.org/10.1111/j.1462-2920.2005.00731.x

Fang, Z., 2011. Theory and application of Thermoelectrochemistry, in: Moreno-Piraján, J.C. (Ed.), Thermodynamics - Physical Chemistry of Aqueous Systems. IntechOpen, London, pp. 27–48. https://doi.org/10.5772/22009

Franks, A.E., Nevin, K.P., Jia, H., Izallalen, M., Woodard, T.L., Lovley, D.R., 2009. Novel strategy for three-dimensional real-time imaging of microbial fuel cell communities: monitoring the inhibitory effects of proton accumulation within the anode biofilm. Energy Environ. Sci. 2, 113–119. https://doi.org/10.1039/b816445b

Fricke, K., Harnisch, F., Schröder, U., 2008. On the use of cyclic voltammetry for the study of anodic electron transfer in microbial fuel cells. Energy Environ. Sci. 1, 144–147. https://doi.org/10.1039/b802363h

Gescher, J., Kappler, A. (Eds.), 2012. Microbial Metal Respiration: From Geochemistry to Potential Applications. Springer, Berlin, Heidelberg.

Heijnen, J.J., Kleerebezem, R., 2010. Bioenergetics of microbial growth, in: Flickinger, M.C. (Ed.), Encyclopedia of Industrial Biotechnology: Bioprocess, Bioseparation and Cell Technology. John Wiley & Sons Inc., pp. 1–24. https://doi.org/10.1002/0471250589.ebt026

Heijnen, J.J., van Dijken, J.P., 1992. In search of a thermodynamic description of biomass yields for the chemotrophic growth of microorganisms. Biotechnol. Bioeng. 39, 833–858. https://doi.org/10.1002/bit.260390806

Hiegemann, H., Littfinski, T., Krimmler, S., Lübken, M., Klein, D., Schmelz, K.G., Ooms, K., Pant, D., Wichern, M., 2019. Performance and inorganic fouling of a submergible 255 L prototype microbial fuel cell module during continuous long-term operation with real municipal wastewater under practical conditions. Bioresour. Technol. 294, 122227. https://doi.org/10.1016/j.biortech.2019.122227

Howley, E., Ki, D., Krajmalnik-brown, R., Torres, C.I., 2022. Geobacter sulfurreducens' unique metabolism results in cells with a high iron and lipid content. bioRxiv 2, 1–6.

Joshi, K., Chan, C.H., Bond, D.R., 2021. Geobacter sulfurreducens inner membrane cytochrome CbcBA controls electron transfer and growth yield near the energetic limit of respiration. Mol. Microbiol. 116, 1124–1139. https://doi.org/10.1111/mmi.14801

Jung, S., Regan, J.M., 2007. Comparison of anode bacterial communities and performance in microbial fuel cells with different electron donors. Appl. Microbiol. Biotechnol. 77, 393–402. https://doi.org/10.1007/s00253-007-1162-y

Koch, C., Harnisch, F., 2016. Is there a Specific Ecological Niche for Electroactive Microorganisms? ChemElectroChem 3, 1282–1295. https://doi.org/10.1002/celc.201600079

Kontogeorgis, G.M., Folas, G.K., 2010. Thermodynamic Models for Industrial Applications: From Classical and Advanced Mixing Rules to Association Theories. John Wiley & Sons, Ltd., Chichester.

Korth, B., Harnisch, F., 2019. Spotlight on the energy harvest of electroactive microorganisms: The impact of the applied anode potential. Front. Microbiol. 10. https://doi.org/10.3389/fmicb.2019.01352

Korth, B., Heber, C., Normant-Saremba, M., Maskow, T., Harnisch, F., 2021. Precious Data from Tiny Samples: Revealing the Correlation Between Energy Content and the Chemical Oxygen Demand of Municipal Wastewater by Micro-Bomb Combustion Calorimetry. Front. Energy Res. 9. https://doi.org/10.3389/fenrg.2021.705800

Korth, B., Kretzschmar, J., Bartz, M., Kuchenbuch, A., Harnisch, F., 2020a. Determining incremental coulombic efficiency and physiological parameters of early stage Geobacter spp. enrichment biofilms. PLoS One 15, e0234077. https://doi.org/10.1371/journal.pone.0234077

Korth, B., Kuchenbuch, A., Harnisch, F., 2020b. Availability of Hydrogen Shapes the Microbial Abundance in Biofilm Anodes based on Geobacter Enrichment. ChemElectroChem 7, 1–6. https://doi.org/10.1002/celc.202000731

Korth, B., Maskow, T., Picioreanu, C., Harnisch, F., 2016. The microbial electrochemical Peltier heat: An energetic burden and engineering chance for primary microbial electrochemical technologies. Energy Environ. Sci. 9, 2539–2544. https://doi.org/10.1039/C6EE01428C

Korth, B., Rosa, L.F.M., Harnisch, F., Picioreanu, C., 2015. A framework for modeling electroactive microbial biofilms performing direct electron transfer. Bioelectrochemistry 106, 194–206.

https://doi.org/10.1016/j.bioelechem.2015.03.010

Kretzschmar, J., Rosa, L.F.M., Zosel, J., Mertig, M., Liebetrau, J., Harnisch, F., 2016. A microbial biosensor platform for in-line quantification of acetate in anaerobic digestion: potential and challenges. Chem. Eng. Technol. 39, 637–642. https://doi.org/10.1002/ceat.201500406

Kubannek, F., Block, J., Munirathinam, B., Krull, R., 2022. Reaction kinetics of anodic biofilms under changing substrate concentrations: Uncovering shifts in Nernst-Monod curves via substrate pulses. Eng. Life Sci. 22, 152–164. https://doi.org/10.1002/elsc.202100088

Kumar, A., Hsu, L.H., Kavanagh, P., Barrière, F., Lens, P.N.L., Lapinsonnière, L., V, J.H.L., Schröder, U., Jiang, X., Leech, D., 2017. The ins and outs of microorganism–electrode electron transfer reactions. Nat. Rev. Chem. 1, 24. https://doi.org/10.1038/s41570-017-0024

Larrosa, A., Lozano, L.J., Katuri, K.P., Head, I., Scott, K., Godinez, C., 2009. On the repeatability and reproducibility of experimental two-chambered microbial fuel cells. Fuel 88, 1852–1857. https://doi.org/10.1016/j.fuel.2009.04.026

Levar, C.E., Chan, C.H., Mehta-Kolte, M.G., Bond, D.R., 2014. An Inner Membrane Cytochrome Required Only for Reduction of High Redox Potential Extracellular Electron Acceptors. MBio 5, e02034-14. https://doi.org/10.1128/mBio.02034-14.Editor

Liu, J.-S., Vojinović, V., Patiño, R., Maskow, T., von Stockar, U., 2007. A comparison of various Gibbs energy dissipation correlations for predicting microbial growth yields. Thermochim. Acta 458, 38–46. https://doi.org/10.1016/j.tca.2007.01.016

Liu, Y., Bond, D.R., 2012. Long-distance electron transfer by G. sulfurreducens biofilms results in accumulation of reduced c-type cytochromes. ChemSusChem 5, 1047–53. https://doi.org/10.1002/cssc.201100734

Logan, B.E., Rabaey, K., 2012. Conversion of wastes into bioelectricity and chemicals by using microbial electrochemical technologies. Science (80-.). 337, 686–690. https://doi.org/10.1126/science.1217412

Logan, B.E., Rossi, R., Ragab, A., Saikaly, P.E., 2019. Electroactive microorganisms in bioelectrochemical systems. Nat. Rev. Microbiol. 1, 307–319. https://doi.org/10.1038/s41579-019-0173-x

Ly, H.K., Harnisch, F., Hong, S.-F., Schröder, U., Hildebrandt, P., Millo, D., 2013. Unraveling the interfacial electron transfer dynamics of electroactive microbial biofilms using surface-enhanced Raman spectroscopy. ChemSusChem 6, 487–92. https://doi.org/10.1002/cssc.201200626

Mahadevan, R., Bond, D.R., Butler, J.E., Coppi, M. V, Palsson, B.O., Schilling, C.H., Lovley, D.R., 2006. Characterization of Metabolism in the Fe (III) -Reducing Organism Geobacter sulfurreducens by Constraint-Based Modeling. Appl. Environ. Microbiol. 72, 1558–1568. https://doi.org/10.1128/AEM.72.2.1558

Malvankar, N.S., Tuominen, M.T., Lovley, D.R., 2012. Biofilm conductivity is a decisive variable for high-current-density Geobacter sulfurreducens microbial fuel cells. Energy Environ. Sci. 5, 5790–5797. https://doi.org/10.1039/c2ee03388g

Molenaar, S., Sleutels, T.H.J.A., Pereira, J., Lorio, M., Borsje, C., Zamudio, J.A., Fabregat-Santiago, F., Buisman, C.J.N., Heijne, A., 2018. In situ biofilm quantification in Bioelectrochemical Systems using Optical Coherence Tomography. ChemSusChem 11, 1–9. https://doi.org/10.1002/cssc.201800589

Morgado, L., Paixão, V.B.B.B., Schiffer, M., Pokkuluri, P.R.R.R., Bruix, M., Salgueiro, C.A., 2012. Revealing the structural origin of the redox-Bohr effect: the first solution structure of a cytochrome from Geobacter sulfurreducens. Biochem. J. 441, 179–187. https://doi.org/10.1042/BJ20111103

Moß, C., Behrens, A., Schröder, U., 2019. The limits of three-dimensionality - Systematic assessment of effective anode macro-structure dimensions for mixed culture electroactive biofilms. ChemSusChem 13, 582–589. https://doi.org/10.1002/cssc.201902923

Nelson, D.L., Cox, M., 2017. Lehninger Principles of Biochemistry, 7th ed. WH Freeman, New York City.

Pereira, J., Mediayati, Y., van Veelen, H.P.J., Temmink, H., Sleutels, T., Hamelers, B., Heijne, A. ter, 2022a. The effect of intermittent anode potential regimes on the morphology and extracellular matrix composition of electro-active bacteria. Biofilm 4, 101028. https://doi.org/10.1016/j.bioflm.2021.100064

Pereira, J., Pang, S., Borsje, C., Sleutels, T., Hamelers, B., ter Heijne, A., 2022b. Real-time monitoring of biofilm thickness allows for determination of acetate limitations in bio-anodes. Bioresour. Technol. Reports 18. https://doi.org/10.1016/j.biteb.2022.101028

Reguera, G., Kashefi, K., 2019. The electrifying physiology of Geobacter bacteria, 30 years on. Adv. Microb. Physiol. 74, 1–96. https://doi.org/10.1016/bs.ampbs.2019.02.007

Roels, J.A., 1980. Application of macroscopic principles to microbial metabolism. Biotechnol. Bioeng. 22, 2457–2514. https://doi.org/10.1002/bit.260221202

Rossi, R., Logan, B.E., 2022. Impact of reactor configuration on pilot-scale microbial fuel cell performance. Water Res. 225, 119179. https://doi.org/https://doi.org/10.1016/j.watres.2022.119179

Sadhukhan, J., Lloyd, J.R., Scott, K., Premier, G.C., Yu, E.H., Curtis, T., Head, I.M., 2016. A critical review of integration analysis of microbial electrosynthesis (MES) systems with waste biorefineries for the production of biofuel and chemical from reuse of CO2. Renew. Sustain. Energy Rev. 56, 116–132. https://doi.org/10.1016/j.rser.2015.11.015

Schink, B., 1984. Fermentation of 2,3-butanediol by Pelobacter carbinolicus sp. nov. and Pelobacter propionicus sp. nov., and evidence for propionate formation from C2 compounds. Arch. Microbiol. 137, 33–41. https://doi.org/10.1007/BF00425804

Schröder, U., Harnisch, F., Angenent, L.T., 2015. Microbial Electrochemistry and Technology: terminology and classification. Energy Environ. Sci. 8, 513–519. https://doi.org/10.1039/C4EE03359K

Schrott, G.D., Bonanni, P.S., Busalmen, J.P., 2019. Open circuit potentiometry reports on internal redox states of cells in G. Sulfurreducens biofilms. Electrochim. Acta 303, 176–182. https://doi.org/10.1016/j.electacta.2019.02.078

Torres, C.I., Krajmalnik-Brown, R., Parameswaran, P., Marcus, A.K., Wanger, G., Gorby, Y.A., Rittmann, B.E., 2009. Selecting anode-respiring bacteria based on anode potential: phylogenetic, electrochemical, and microscopic characterization. Environ. Sci. Technol. 43, 9519–9524. https://doi.org/10.1021/es902165y

VanBriesen, J.M., 2002. Evaluation of methods to predict bacterialyield using thermodynamics. Biodegradation 13, 171–190. https://doi.org/10.1023/A:1020887214879

von Stockar, U., 2018. Biothermodynamics: Bridging Thermodynamics with Biochemical Engineering. J. Chem. Educ. Res. Pract. 2, 1–7.

von Stockar, U., von der Wielen, L.A.M., 2003. Back to Basics: Thermodynamics in Biochemical Engineering, in: et al. (Ed.), Process Integration in Biochemical Engineering, Advances in Biochemical Engineering/Biotechnology, Vol. 80. Springer, Berlin, Heidelberg, pp. 1–17.

Zacharoff, L.A., Chan, C.H., Bond, D.R., 2016. Reduction of low potential electron acceptors requires the CbcL inner membrane cytochrome of Geobacter sulfurreducens. Bioelectrochemistry 107, 7–13. https://doi.org/10.1016/j.bioelechem.2015.08.003